Experimental validation of GNPy in a multi-vendor flex-grid flex-rate WDM optical transport scenario

Experimental validation of GNPy in a multi-vendor flex-grid flex-rate WDM optical transport scenario

ANDREA D'AMICO[1,*], ELLIOT LONDON[1], BERTRAND LE GUYADER[2], FLORIAN FRANK[2], ESTHER LE ROUZIC[2], ERWAN PINCEMIN[2], NICOLAS BROCHIER[2], AND VITTORIO CURRI[1]

[1] Politecnico di Torino, Corso Duca degli Abruzzi, 24, Torino, Italy
[2] Orange Labs, 22300 Lannion, France
[*] Corresponding author: andrea.damico@polito.it

Compiled April 8, 2022

We experimentally test the accuracy of a quality of transmission estimator within a laboratory flex-grid flex-rate framework, considering 8 multi-vendor transceivers (TRXs) with symbol rates ranging from 33 to 69 Gbaud, variable constellations (QPSK, 8-QAM and 16-QAM PCS), for data rates of 100 Gbit/s up to 300 Gbit/s, and a flex-grid wavelength division multiplexed (WDM) spectrum, with channel spacings of 50 and 75 GHz. As a QoT-E we utilize an enhanced implementation of the open-source GNPy project. We demonstrate that this QoT estimator provides a high level of accuracy in generalized signal-to-noise ratio (GSNR) computation, with an average error value not exceeding 0.5 dB, for the scenario under investigation. These values are computed with respect to the measured bit-error ratio (BER) converted to the GSNR using the TRX model obtained via back-to-back characterization. These results demonstrate that the optimal management of flex-grid flex-rate WDM optical transport arises by managing power spectral densities instead of power per channel, as in traditional fixed-grid systems.

http://dx.doi.org/10.1364/ao.XX.XXXXXX

1. INTRODUCTION

The continually-increasing demand for data transport [1], specifically from transparent wavelength division multiplexed (WDM) optical networks [2], has spurred research into a wide variety of forward-thinking solutions to address this problem using existing infrastructures. To surpass existing capacity limits, new standards and approaches have emerged, ranging down from the component and physical-layer up to top-level optical data planning control and management.

WDM optical transport based on dual-polarization coherent optical technologies is fast evolving; transparent fiber transmission with rigid spectral implementations based on fixed WDM grids and fixed-rate transceivers (TRXs) are moving towards flex-grid [3] WDM implementations and flex-rate TRXs. Thanks to innovations in silicon photonic technologies [4] and photonic integrated circuits, the TRX symbol rate, R_s, now exceeds 60 Gbaud in commercial products and transmission beyond 100 Gbaud has been demonstrated in laboratory prototypes [5]. Moreover, multi-subcarrier solutions are proposed and commercially available as an alternative method of further increasing transmission capacity [6]. Through the use of high cardinality signal constellations such as 64-QAM, optical interfaces up to 800 Gbit/s are now possible, with transmission beyond 1 Tbit/s expected to become a commercial reality in the near future. Furthermore, hybrid modulation formats [7] and/or probabilistic shaped constellations (PSC)s [8] allow data rates to be tuned seamlessly, enabling optimal quality-of-transmission (QoT) exploitation upon the available transparent lightpaths (LP)s. Besides the traditional closed approach, disaggregated and possibly open WDM solutions are emerging with the introduction of white-boxes and pluggable TRXs [9]. The result of these advances is that operators are now envisioning the evolution towards progressive deployment of disaggregated solutions [10, 11].

This scenario provides the foundation for a software-defined networking (SDN) implementation that encompasses the WDM transport layer [12] by implementing open-control network element (NE) interfaces for an optical control plane that operates in a multivendor scenario. Several consortia are actively working to further develop and standardize these advances to define open protocols, data structures and application programming interfaces (APIs). In particular, the Telecom Infra Project (TIP) develops open hardware and software solutions for open network infrastructures, and the OpenROADM consortium [13] works to standardize re-configurable optical add/drop multiplexer (ROADM) models for networking scenarios where ROADM-to-ROADM amplified links are independent and possibly open WDM optical line systems (OLSs). Recently, the implementation agreement (IA) for fixed-rate 400G-ZR optical interfaces has been released by the Optical Internetworking Forum (OIF) [14].

A corresponding IA for flex-rate 400G-ZR+ implementations is currently under development, along with 800 Gbit/s solutions. Disaggregated transponders providing these TRX configurations are commercially available, along with open solutions that have been proposed by the TIP [15] – these technologies will steer the progression towards multi-vendor disaggregated and open optical infrastructures, which will potentially be shared by multiple operators and have a WDM optical transport that will be a fully virtualized network function.

To pursue this objective, the fundamental request by network operators is that the QoT of a TRX over a transparent LP may be computed, for a provided transport network model and status. When working with dual-polarization coherent optical technologies, it has been extensively demonstrated that propagation over a transparent LP is well modeled by an additive white and Gaussian noise (AWGN) nonlinear channel, with a corresponding QoT fully quantified by the generalized optical signal-to-noise ratio (GSNR) [16, 17]. The GSNR includes the two Gaussian disturbances that impair the received constellation: the accumulated ASE noise from the amplifiers and the nonlinear interference (NLI) introduced by nonlinear crosstalk. From TRX back-to-back characterization the GSNR can be related to the pre-forward error correction (FEC) BER [18, 19]. By doing so, the BER threshold requested by the FEC technology and modulation format corresponds to a unique GSNR threshold. Combined with the spectral occupancy given by the channel symbol rates and roll-off values, the fundamental QoT and bandwidth requests from the TRX for a given LP can be quantified [20]. Throughout this work we express all signal-to-noise ratios by considering the noises integrated over each distinct channel bandwidth, instead of a fixed 0.1 nm bandwidth. This perspective is considered in order to better observe the spectral efficiency in terms of a GSNR degradation, as this quantity does not depend upon the channel symbol rates.

Virtualization of the WDM transport layer is enabled by a QoT estimator (QoT-E) that evaluates the GSNR on a selected LP, given the network topology, NE models and network loading status [21]. The TIP consortium develops an open-source library named GNPy [22] that follows this approach for design, planning, control and management of disaggregated optical networks. GNPy has been extensively tested in multi-vendor scenarios in both green-field and brown-field commercial infrastructures. Thus far, experimental results have demonstrated that GNPy is capable of predicting GSNR to a high degree of accuracy in 50 GHz fixed-grid scenarios, with fixed symbol rates and purely dual-polarization QPSK, 8-QAM and 16-QAM constellations, for 100, 150 and 200 Gbit/s data rates [23–25]. Concerning flex-grid flex-rate scenarios, experimental verification for GNPy and other QoT-Es has in general been limited – we highlight that a preliminary test of GNPy for flex-grid flex-rate transmission has been presented in [26].

In this work, we extend the analysis performed in [26] by considering 8 multi-vendor TRXs, with symbol rates ranging from 33 to 69 Gbaud, TRX constellations of QPSK, 8-QAM and PCS-16-QAM, for data rates ranging from 100 Gbit/s up to 300 Gbit/s, along with a flex-grid WDM configurations with channel spacings of 50 and 75 GHz. This experimental transmission has been performed upon a bandwidth of 3 THz in the C-band, with the remaining spectrum aside from these TRXs fully loaded with standard 100 Gbps channels. This experiment has been carried out through a point-to-point 20-span OLS located at Orange Labs, Lannion, France, with the laboratory setup shown in Fig. 1. We present the experimental results along with those corresponding to the GNPy model, including estimations for the interval of confidence, showing that the QoT prediction given by GNPy has an average error value that does not exceed 0.5 dB for every considered TRX. Besides confirming the reliability of GNPy as a vendor-neutral software model for WDM optical transport, we also show that the optimal management of flex-grid flex-rate OLSs is enabled by managing power spectral densities, $P_{ch,i}/R_{s,i}$, instead of power per channel, $P_{ch,i}$, as is used in fixed-grid management. This approach has been previously suggested and investigated for flex-grid transmission scenarios in [27, 28].

The rest of this work is divided as follows: within Sec. 2 we explain the features and topology of disaggregated networks, such as the one investigated within this work. In Sec. 3 we give a detailed description of the experimental setup used for flex-grid flex-rate transmission and the measurements that have been performed. In Sec. 4 we describe the model implementations used within this work, with both the $\mathrm{SNR_{NL}}$ and OSNR contributions to the GSNR estimated using an enhanced implementation of the open-source GNPy library. We then compare our predictions to the experimental results, initiating a discussion on key differences between the investigated use case and fixed-grid networks which must be taken into account. Finally, in Sec. 5 we provide a summary of the paper.

Fig. 1. An image of the experimental setup within Orange Labs in Lannion, France.

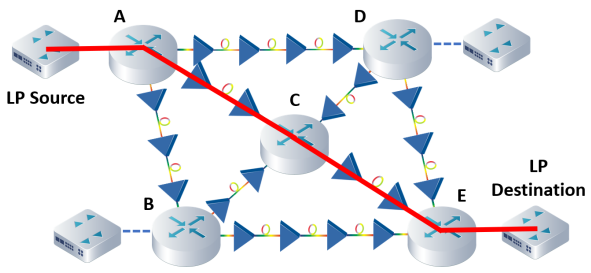

Fig. 2. An example of the architecture of a partially disaggregated optical network. In this scenario LPs are routed through open ROADMs located at OLS terminations between a given source and destination.

2. NETWORK ARCHITECTURE

Within this work, we consider a partially disaggregated optical network framework, as depicted in Fig. 2, with top-level management performed by an optical network controller (ONC), where the amplified lines connecting ROADMs may be independent WDM OLSs [10, 29, 30]. In this scenario, the ROADMs are disaggregated [13, 31], meaning that each degree unit, including the wavelength selective switches (WSS)s, are the ingress/egress of an independent OLS. Each OLS is managed by an independent optical line controller (OLC) that is responsible for setting optical power levels by controlling the in-line, pre-amp and booster amplifiers. The ONC is in charge of deploying LPs, meaning that once the available wavelength and route has been defined by the routing wavelength and spectrum assignment algorithm (RWSA), the LP QoT must be computed to properly control the TRX. By comparing the available GSNR to the TRX model (the GSNR threshold from back-to-back characterization), the ONC defines feasible symbol rates and modulation formats (and probabilistic constellation shaping (PCS) settings in case of flex-rate TRXs), finding the overall LP feasibility [13, 32–34]. As the LPs are modelled as AWGN nonlinear channels, the QoTs of the LPs are the accumulated GSNRs from the source, s, to the destination, d, for each transparent LP crossing multiple OLSs. According to a disaggregated approach to QoT computation [35], the LP GSNR for any given channel under test (CUT) is given by:

$$\mathrm{GSNR}_{sd} = \frac{1}{\sum_i \mathrm{GSNR}_i^{-1}}, \quad (1)$$

where GSNR_i is the GSNR for the ith crossed OLS:

$$\mathrm{GSNR}_i = \frac{P_{\mathrm{CUT},i}}{P_{\mathrm{ASE},i} + P_{\mathrm{NLI},i}} = \frac{1}{\mathrm{OSNR}_i^{-1} + \mathrm{SNR}_{\mathrm{NL},i}^{-1}}, \quad (2)$$

where $P_{\mathrm{CUT},i}$ is the CUT power at the ith OLS egress, $P_{\mathrm{ASE},i}$ and $P_{\mathrm{NLI,i}}$ are the accumulated ASE and NLI noises on the ith OLS impairing the receiver decision variable, respectively. The effects of the two disturbances are quantified by the two GSNR components: the optical signal-to-noise ratio, $\mathrm{OSNR}_i = P_{\mathrm{CUT},i}/P_{\mathrm{ASE},i}$, and the nonlinear signal-to-noise ratio, $\mathrm{SNR}_{\mathrm{NL},i} = P_{\mathrm{CUT},i}/P_{\mathrm{NLI},i}$. As each OLS is controlled independently, to compute the overall GSNR_{sd}, it is crucial to be able to accurately evaluate each GSNR_i.

A QoT-E must reliably evaluate both GSNR components, meaning that an accurate model for the losses of each WDM wavelength, as well as the amplifier gain and ASE noise contributions are required in order to properly evaluate the $\mathrm{SNR}_{\mathrm{NL}}$ and OSNR components, respectively. Ideally, for $\mathrm{SNR}_{\mathrm{NL}}$ computation the QoT-E evaluates the NLI noise using a disaggregated approach [36], and considers the interactions between the NLI generation and the spatial and frequency dependency of the total fiber loss profile given by the intrinsic fiber loss, that can vary significantly along frequency [37, 38], and the effects of Stimulated Raman Scattering (SRS) [39, 40].

A vendor-neutral QoT-E operated by a ONC must be able to communicate with the OLC that provides the line description, i.e., the information regarding the fiber spans (lengths, chromatic dispersion values, nonlinearity coefficients, losses) and the amplifiers (gains, noise figures, tilts). Besides this line description, each OLC supplies information regarding the spectral loading of the ith OLS, and the corresponding GSNR_i. Given a GSNR_{sd} and the TRX GSNR threshold, an optimized control of the modulation format (or shaping in case of PCS) can be implemented – within this framework minimizing the system margin fundamentally depends upon the accuracy of the QoT-E.

3. EXPERIMENTAL SETUP

Fig. 3 includes a detailed description of the experimental setup assembled at Orange Labs which has been used to measure various QoT transmission metrics in a flex-grid flex-rate scenario. The OLS under consideration is composed of 20×80 km spans of ITU.T G.652 fiber with an average loss of 16.6 dB, dispersion values of 16.7 ps / (nm·km) and effective areas of 80 μm^2, both evaluated at a reference wavelength of 1550 nm. After each fiber span, a JDSU WRA 200 erbium doped fiber amplifier (EDFA) is placed and operated in a constant gain mode in order to fully

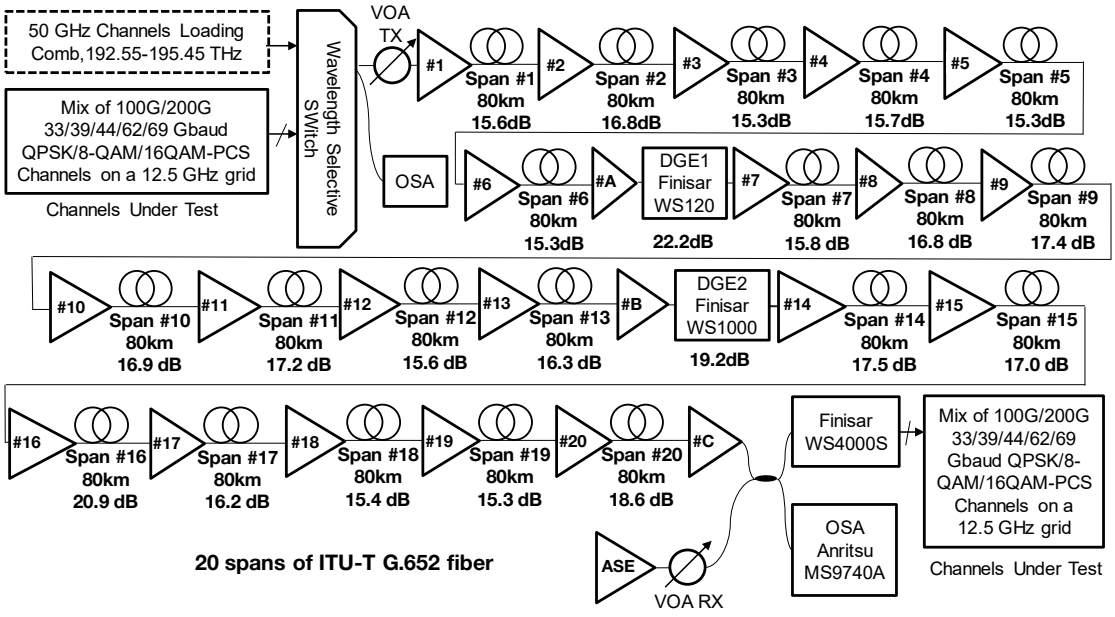

Fig. 3. A flow diagram providing a representation of the optical line used for transmission within this experiment.

recover the fiber loss. In order to compensate for stimulated Raman scattering (SRS) effects, each EDFA gain tilt has been set so that 1 dB of tilt over the spectrum bandwidth is recovered for each span. After the 6th and 13th spans two dynamic gain equalizers (DGEs) are used to equalize the spectrum, compensating for ripples due to the amplification process and for residual tilt caused by the SRS.

Regarding transmission, two different spectra have been propagated and analysed, for a total bandwidth that occupies a portion of the C-band located between 192.55 THz (1556.96 nm) and 195.45 THz (1533.86 nm). In both cases, we consider a total of 55 channels organized in a flexible WDM grid with a minimum division of 12.5 GHz. The overall bandwidth, along with the distinct propagated channels, can be schematically divided in two sub-regions:

- A 50 Hz fixed-grid loading comb composed of 47 QPSK-modulated 100 Gbit/s channels with symbol rates of 28 and 33 Gbaud;
- A sub-region of interest located between 192.95 THz (1553.73 nm) and 193.45 THz (1549.48 nm) that includes a total of 8 CUTs:
  - two QPSK 100 Gbit/s channels with symbol rates of 33 Gbaud;
  - three 16-QAM 200 Gbit/s channels with symbol rates of 39 Gbaud;
  - one 8-QAM 200 Gbit/s channel with a symbol rate of 44 Gbaud;
  - one 16-QAM 300 Gbit/s channel with a symbol rate of 62 Gbaud;
  - one QPSK 200 Gbit/s channel with a symbol rate of 69 Gbaud.

For this experimental investigation, the loading comb and two distinct CUT spectral combinations have been multiplexed using a WSS to create two distinct spectral configurations.

In this article, we refer to the two spectra as the *adjacent* and *far apart* spectral configurations, described in detail in Tab. 1. The main difference between the two analysed spectra is that the two CUTs with the larger symbol rates, 62 and 69 Gbaud, are placed next to each other or with other CUTs between them; Fig. 4 includes a visual representation of these two configurations. We choose these two configurations in order to observe any variation upon the GSNRs within the spectral region of interest when the channels with the largest symbol rates change spectral occupations. If GSNR variations are present, they must be taken into account by the ONC when optimizing the configuration of the channels with respect to their symbol rates.

Both spectra have been transmitted at various launch powers and, at the OLS termination, the CUTs have been demultiplexed with a Finisar WaveShaper 4000S and then received, allowing QoT analysis. In particular, the launch powers for each channel have been set such that an approximately uniform power spectral density (PSD) is attained over the entire bandwidth; this is performed by maintaining the ratio between the launch powers of any couple of distinct channels equal to the ratio between their symbol rates, which is also visible in Fig. 4. In order to observe the GSNR variation as the optimal power level is approached, we retain this uniform PSD and perform a power sweep, varying the equivalent power per channel, $\overline{P}_{\mathrm{ch}}$, between -2 and 2 dBm in 0.5dB increments, where $\overline{P}_{\mathrm{ch}}$ is defined as the total signal power divided by the total number of channels.

In this framework, for each transmitted signal, we measured the BER at the receiver and the OSNR at the OLS termination for each CUT. In particular, the OSNR values are obtained from two distinct signal power measurements and the ASE noise after the last EDFA. The ASE noise power has been measured by switching off each CUT in turn and then evaluating the noise floor within the relative bandwidth. Both of these power measurements have been performed using a MS9740A Anritsu optical spectrum analyzer (OSA); in Fig. 5 an example of the transmitted signal power is shown.

In order to compare the performance of the CUTs to the predictions given by GNPy, the measured BERs have to be converted to GSNR values. This conversion also has the benefit of decorrelating the measurements to the specific characteristics of each distinct TRX. Furthermore, it enables a direct analysis of the relation between the QoT and the physical layer features of the investigated system and is crucial in enabling the ONC to

Table 1. The *adjacent* and *far apart* spectral configurations: 75 GHz and 300 GHz spacing between the 62 and 69 Gbaud carriers, respectively. These carriers are shown in bold and the loading comb is shown in italics.

adjacent spectral configuration								
f_0	*192.55–192.9*	192.975	193.05	193.125	**193.2**	**193.275**	193.35, 193.4, 193.45	*193.55–195.45*
N_{ch}	*8*	1	1	1	**1**	**1**	3	*39*
R_s [Gbaud]	*33*	33	33	44	**62**	**69**	39	*33*
M	*QPSK*	QPSK	QPSK	8-QAM	**16-QAM PCS**	**QPSK**	16-QAM PCS	*QPSK*
R_b [Gbit/s]	*100*	100	100	200	**300**	**200**	200	*100*

far apart spectral configuration								
f_0	*192.55–192.9*	**192.975**	193.05	193.125	193.2	**193.275**	193.35, 193.4, 193.45	*193.55–195.45*
N_{ch}	*8*	**1**	1	1	1	**1**	3	*39*
R_s [Gbaud]	*33*	**62**	33	44	33	**69**	39	*33*
M	*QPSK*	**16-QAM PCS**	QPSK	8-QAM	QPSK	**QPSK**	16-QAM PCS	*QPSK*
R_b [Gbit/s]	*100*	**300**	100	200	100	**200**	200	*100*

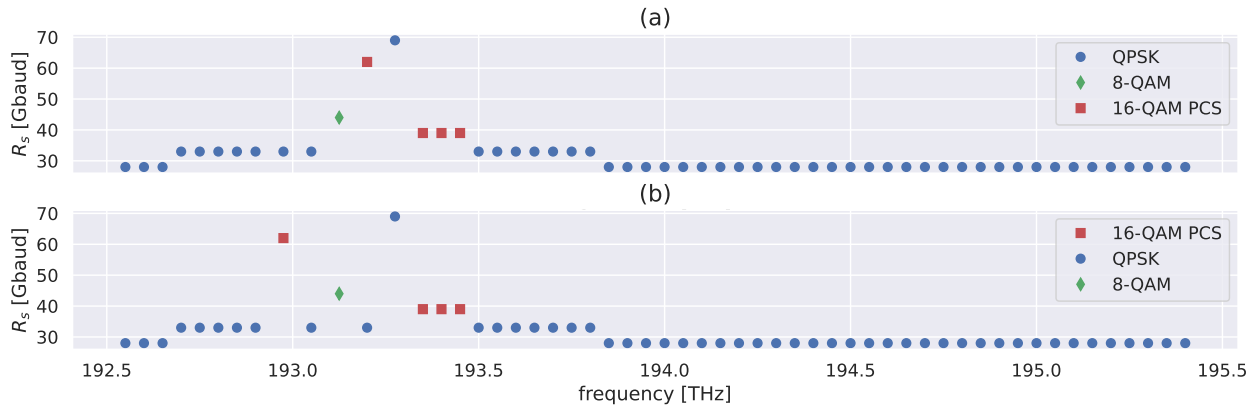

Fig. 4. Visualization of the (a) *adjacent* and (b) *far apart* spectral configurations, as fully described in Tab. 1.

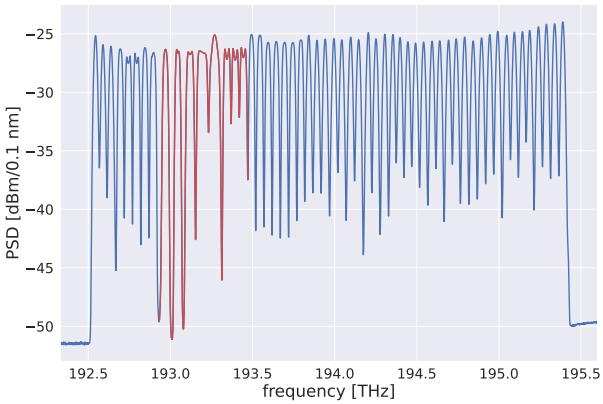

Fig. 5. Optical spectrum at the OLS input; the spectral region of interest where the CUTs are located is highlighted in red.

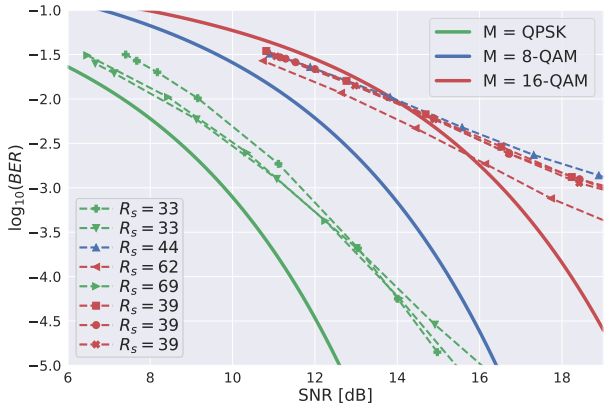

Fig. 6. Back-to-back characterization for each distinct channel within this experimental campaign; continuous and dashed lines represent the theoretical and measured back-to-back curves, respectively. The channel symbol rates, R_s, are given in Gbaud

perform an optimal symbol rate and modulation format setting.

The first required step to convert from BER to GSNR is the back-to-back characterization of every CUT TRX. These back-to-back characterizations have been performed by measuring the BER and the OSNR (which, in this case, is equal to the GSNR) with an increasing level of ASE noise loading. In Fig. 6, the theoretical expectations for the different modulation formats are compared with the measured back-to-back characterizations. The detachment between the theoretical and measured curves is due to additional implementation-specific degradations that are not related to the LP QoT. When the GSNR increases significantly, the additional noise components due to electrical components and analog-to-digital converter (ADC) quantization in the receiver are no longer negligible. We note that the back-to-back characterizations of the 16-QAM-PCS-modulated channels behave the same as the 8-QAM-modulated channel, as their constellation is reshaped into an equivalent 8-QAM modulation format. We stress that the GSNR is expressed by considering the entire channel bandwidths as noise reference bandwidths, rather than a 0.1 nm bandwidth. If this method is used, back-to-back performance curves, as expected, are grouped according to the modulation format, regardless of the symbol rate.

At this stage, as the pre-FEC BER is a parameter provided by the TRXs, which are commercial devices with limited access to the internal digital signal processing (DSP) unit, it has not been possible to properly estimate the error on the BER measurements and the consequent confidence interval in GSNR conversions. Properly estimating this quantity would allow a more precise analysis of the QoT investigation with a more accurate description of the system margin and will be the focus of further studies. In order to reasonably quantify the inaccuracies related to the indirect measurement of the GSNR, we assume an error corresponding to a rigid shift in the OSNR measurements up to a maximum ± 0.2 dB, providing a confidence interval, ε, of the derived GSNR values.

Following this back-to-back characterization for each CUT, the BER measurements can be directly converted to GSNR values and compared to the predictions provided by GNPy. Furthermore, the OSNR measurements obtained by the OSA provide an indirect evaluation of the $\mathrm{SNR_{NL}}$ degradation, as a subtraction estimate, which allows a deeper insight in the QoT estimation analysis. A schematic of this procedure applied to a specific CUT is shown in Fig. 7

4. RESULTS AND ANALYSIS

An implementation of the open-source GNPy library has been modified in order to allow variable WDM grid spacings and variable channel settings, such as channel-dependent input powers and symbol rates. Moreover, taking advantage of GNPy's

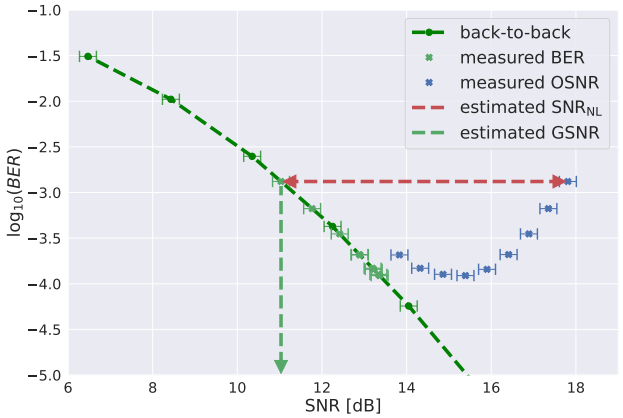

Fig. 7. Schematic of the GSNR and SNR$_{NL}$ evaluation procedure using the values for back-to-back characterization, measured BER and OSNR for the 69 Gbaud CUT.

disaggregated structure, we have improved the NLI estimator by including a variable accumulation coefficient of the self-phase modulation component of the NLI, taking into account the span-by-span coherency dependence upon fiber variety and spectral characteristics [41]. These improvements allow the GNPy engine to adequately simulate the investigated experimental testbed that includes the propagation of flex-grid flex-rate spectral configurations. In general, the generalized GN model implemented in GNPy provides accurate results when a precise evaluation of the physical layer parameters is available, as it has been extensively shown in previous fixed-grid experiments [16, 24, 25]. For the experimental setup under investigation some physical parameters involve a certain level of uncertainty, or are completely unknown. Among these variables, the EDFA noise figure and the fiber input connector losses, l_c, for each span are fundamental for an accurate system simulation to be achieved. In particular, the former quantity is necessary for an adequate prediction of the OSNR, whereas the input connector loss crucially affects the actual amount of power that is propagated through the fiber; both the SRS power tilt and the generated NLI noise strongly depend on the input power [25]. The EDFA noise figure for each span has been estimated from a single measurement of the OSNR at the OLS termination, with the total launch power set such that $\overline{P}_{\text{ch}} = 2$ dBm. These measurements can be converted to an equivalent noise figure that has been equally redistributed for each span and also partially includes effects due to EDFA ripple. Regarding input connector loss, it is not possible to directly measure or estimate this value from an overall system metric in the same way as we have performed for the noise figure. Therefore, to accommodate uncertainty due to these unknown input connector loss values, we include a confidence interval of 0.25 dB $\pm$ 0.25 dB for each span for the SNR$_{NL}$ and GSNR predictions. We then repeat the GNPy simulations with 0 and 0.5 dB connector loss values, referring to these as the *lower* and *upper* extreme simulation cases, respectively.

The results obtained using these estimations are compared to the measured pre-FEC BER converted to the GSNR, along with the measured OSNR and the SNR$_{NL}$ obtained by subtraction of the inverse GSNR and OSNR. These results are shown in Fig. 8 for a subset of the CUTs: we include the best and the worst case scenario CUTs in terms of average GSNR prediction accuracy, and the CUTs with symbol rates of 44 and 69 Gbaud. In general, the GNPy engine provides very accurate predictions of the OSNR for all CUTs and launch powers explored in the power sweep. As expected, the generalized GN model implemented in GNPy provides conservative SNR$_{NL}$ predictions for almost all CUTs and $\overline{P}_{\text{ch}}$ values. We highlight that, by increasing $\overline{P}_{\text{ch}}$, the predicted and measured SNR$_{NL}$ values for all cases monotonically decrease and reach the same asymptotic slope, which demonstrates that the model under investigation provides a good representation of the underlying physical phenomena. On the other hand, the SNR$_{NL}$ measurements follow this trend less consistently at low $\overline{P}_{\text{ch}}$ values. Nevertheless, these deviations from the trend can be justified bearing in mind that the SNR$_{NL}$ measurements have been obtained by subtracting the inverse OSNR from the inverse GSNR. As a consequence, the measured SNR$_{NL}$ includes also all the additional SNR degradations that are not included in the system abstraction. Therefore, this deviation can be explained by a constant additional degradation that is more evident at large SNR$_{NL}$ values and becomes negligible as the NLI increases. Furthermore, we observe that the the SNR$_{NL}$ predictions for the CUT with the highest symbol rate, 69 Gbaud, are slightly optimistic for all $\overline{P}_{\text{ch}}$ values. This is due to this particular CUT having a received power that is below the optimal transceiver power range.

To summarize, GNPy provides a conservative prediction with a satisfactory level of accuracy of the total GSNR for every CUT, for all $\overline{P}_{\text{ch}}$ values explored in the power sweep, with the exception of the 69 Gbaud channel, which suffers from additional impairments due to an insufficient received power. A quantitative estimation of the prediction accuracy can be obtained by inspecting the mean, μ, and root mean square (RMS), σ, of the errors in the GSNR simulations, ΔGSNR, defined explicitly in the following expressions:

$$\begin{aligned}
\Delta\text{GSNR} &= \text{GSNR}^{\text{meas}} - \text{GSNR}^{\text{pred}}\big|_{l_c=0.25}\,; \\
\Delta\text{GSNR}_{lower} &= \text{GSNR}^{\text{meas}} - \text{GSNR}^{\text{pred}}\big|_{l_c=0}\,; \\
\Delta\text{GSNR}_{upper} &= \text{GSNR}^{\text{meas}} - \text{GSNR}^{\text{pred}}\big|_{l_c=0.5}\,.
\end{aligned}$$

Both μ and σ are evaluated separately on the *adjacent* and *far apart* spectral configurations as:

$$\begin{aligned}
\mu &= \text{E}\left[\Delta\text{GSNR}\right], \\
\mu_{lower} &= \text{E}\left[\Delta\text{GSNR}_{lower}\right], \\
\mu_{upper} &= \text{E}\left[\Delta\text{GSNR}_{upper}\right]; \qquad \textbf{(3)} \\
\sigma &= \sqrt{\text{E}\left[\left(\Delta\text{GSNR}\right)^2\right]}, \\
\sigma_{lower} &= \sqrt{\text{E}\left[\left(\Delta\text{GSNR}_{lower}\right)^2\right]}, \\
\sigma_{upper} &= \sqrt{\text{E}\left[\left(\Delta\text{GSNR}_{upper}\right)^2\right]}; \qquad \textbf{(4)}
\end{aligned}$$

where the operator E[·] is the average over the entire set of measurements/predictions. These results are reported in Tab. 2, along with the minimum ΔGSNR, which represent the worst-case scenario; here, GNPy provides a non conservative prediction, which also provides a rough estimation of the required QoT-E margin. Moreover, the uncertainties, ϵ, reported in Tab. 2

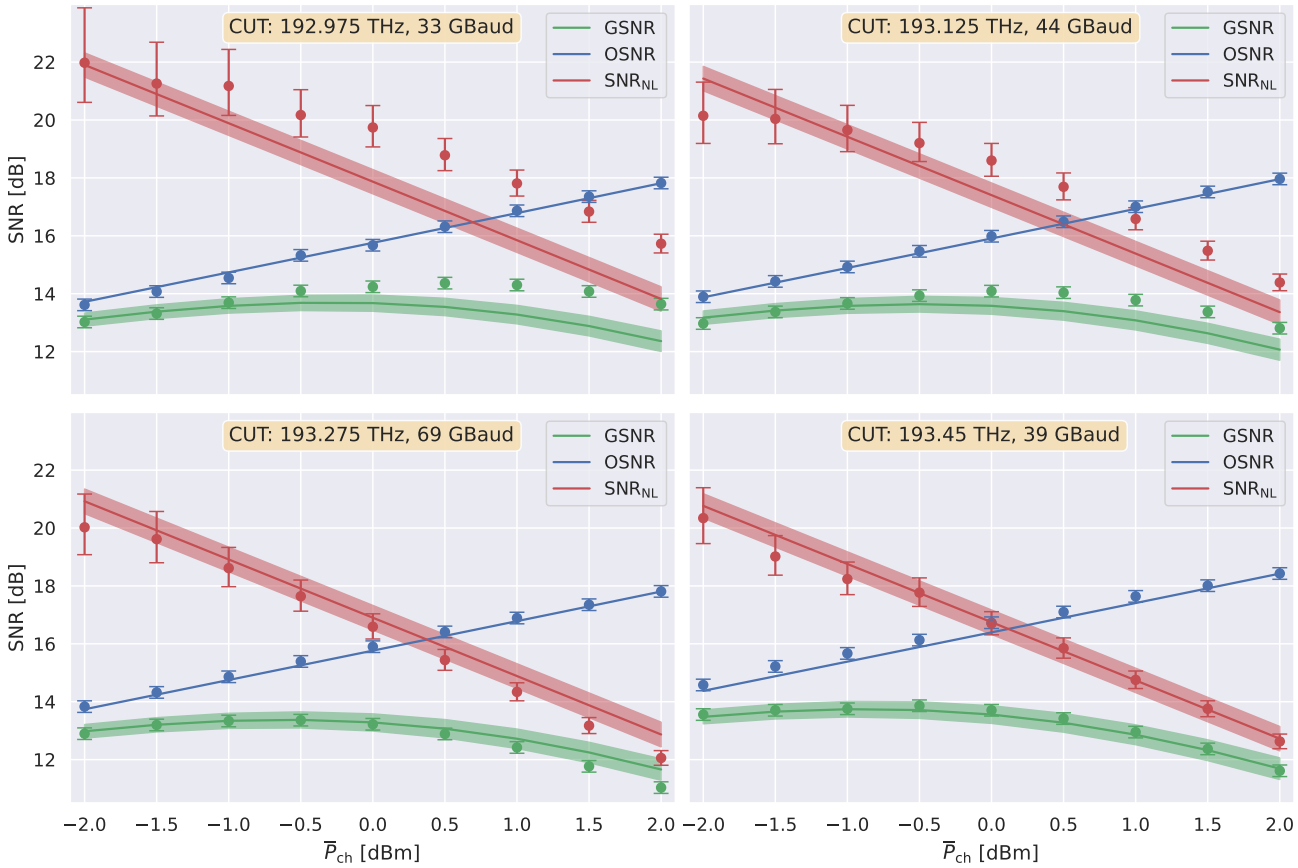

Fig. 8. The dots and the continuous lines represent, respectively, the measured and predicted GSNRs, OSNRs and $\mathrm{SNR_{NL}}$s for 4 selected CUTs in the *adjacent* spectral configuration case, for every explored $\overline{P}_{\mathrm{ch}}$ value. The shaded areas include the confidence interval obtained with the *upper* and *lower* simulations involving the extreme values of the input connector loss.

Table 2. Overall GNPy accuracy defined by means of μ, σ and the minimum value of the GSNR error, ΔGSNR. These results include both spectral configurations and the simulation extremes with respect to input connector losses. Uncertainties, $\pm\epsilon$, are provided for all values.

	adjacent	*far apart*
μ	0.2 ± 0.2 dB	0.1 ± 0.2 dB
σ	0.4 ± 0.1 dB	0.3 ± 0.1 dB
min(ΔGSNR)	-0.6 ± 0.9 dB	-0.8 ± 0.9 dB
μ_{lower}	0.4 ± 0.2 dB	0.3 ± 0.2 dB
σ_{lower}	0.6 ± 0.1 dB	0.5 ± 0.1 dB
$\mathrm{min}(\Delta\mathrm{GSNR}_{lower})$	-0.3 ± 0.9 dB	-0.5 ± 0.9 dB
μ_{upper}	0.1 ± 0.2 dB	-0.1 ± 0.2 dB
σ_{upper}	0.3 ± 0.1 dB	0.3 ± 0.1 dB
$\mathrm{min}(\Delta\mathrm{GSNR}_{upper})$	-0.9 ± 0.9 dB	-1.1 ± 0.9 dB

have been calculated as follows:

$$\begin{aligned}\varepsilon_{\mathrm{min}} &= \varepsilon_{\mathrm{min}(\mathrm{GSNR}^{meas})}\,;\\ \varepsilon_{\mu} &= \sqrt{\mathrm{E}\left[(\varepsilon_{\mathrm{GSNR}^{meas}})^2\right]}\,;\\ \varepsilon_{\sigma} &= \frac{1}{\sigma}\sqrt{\frac{1}{N}\mathrm{E}\left[(\Delta\mathrm{GSNR}^{meas}\cdot\varepsilon_{\mathrm{GSNR}^{meas}})^2\right]}\,,\end{aligned}$$

where N is the total number of measurements/predictions.

In general, GNPy provides very accurate (low value of σ) and unbiased (low value of μ) predictions, with the *upper* simulation providing the most precise estimations. On the other hand, the *lower* simulation provides a more reliable estimation, as the GSNR error on the worst-case scenario is more than halved with respect to the other simulations. These two simulations represent scenarios where either a more accurate or more reliable model may be chosen, depending upon the requirements of the network operator.

These results can be further analysed from an application standpoint by investigating the optimal launch power and GSNR feasibility when higher-cardinality modulation formats are used. In general, the optimal launch power is an implementation-dependent quantity and can be described with different definitions. However, a per-channel power optimization is not straightforward due to the nonlinear effects (both the SRS and NLI) that are generated during fiber propagation. Managing the NLI impairment can be simplified by considering the following heuristic idea: the NLI noise generated by the signal power contained in an infinitesimal bandwidth of an interfering channel does not depend upon the channel itself. We elucidate this idea with an example; the NLI generated by two interfering channels with symbol rates of 33 Gbaud is not significantly different from the NLI generated by one interfering channel with a 66 Gbaud symbol rate, if each of these channels occupy the same frequency slot width.

In a realistic use case, the optimal launch power can therefore

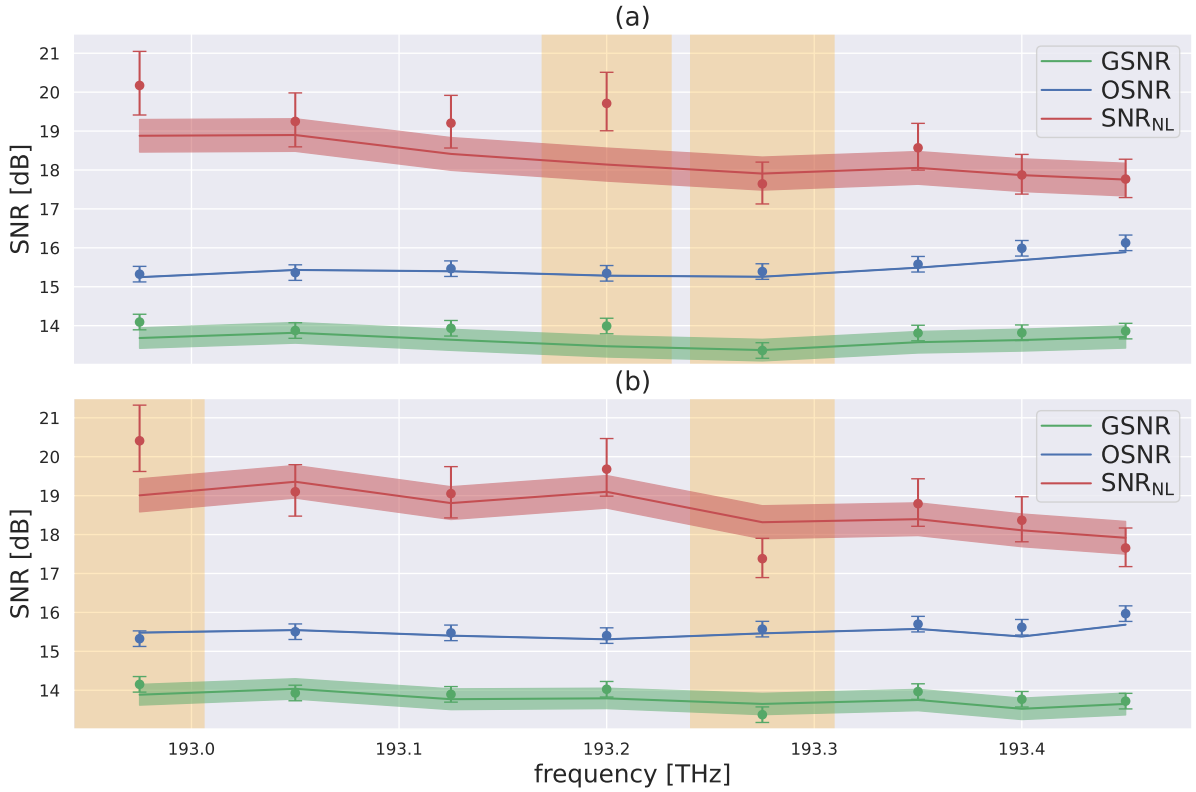

Fig. 9. The dots and the continuous lines represent, respectively, the measured and predicted GSNR, OSNR and $\mathrm{SNR_{NL}}$ for all CUTs. The top and the bottom report the results for the (a) *adjacent* and (b) *far apart* spectral configurations, at the optimal measured working point $\overline{P}_{\mathrm{ch}} = -0.5\,\mathrm{dBm}$. The shaded horizontal areas include the confidence interval obtained with the *upper* and *lower* simulations involving the extreme values of the input connector loss. The largest symbol rate CUTs, 62 and 69 Gbaud, are highlighted with the vertical yellow shades on the left- and right-hand sides respectively.

be defined globally, where an optimization algorithm varies the offset and tilt of a uniform PSD configuration over the entire transmitted spectrum. This constant PSD configuration can then be tilted in order to recover the residual tilt due to uncompensated SRS. Defining a global optimal launch power using this uniform PSD leads to a uniform GSNR distribution for all channels; this reduces management complexity and allows system margins to be kept under control. We remark that the optimization procedure used within this work does not require any additional equipment, as the optimal launch power configuration can be obtained by varying the EDFA gains (or output power) and tilts, which are parameters that are readily accessible in currently deployed infrastructures.

This assumption is, in any case, an oversimplification of the NLI effect and further analysis is required to reach a formal and accurate description. Additionally, we highlight that a more elaborate PSD distribution which takes into account all symbol rate variances within the spectrum can provide a better optimization, however in this analysis we give priority to maintaining a lower level of complexity for ease of optimization management in a realistic use case.

In this work an analysis on the optimal launch power can only partially be performed, as the CUTs occupy a limited portion of the entire spectrum bandwidth. To define the optimal launch power, first we recap that $\overline{P}_{\mathrm{ch}}$ is defined as the total signal power divided by the total number of channels. Secondly, distinct $\overline{P}_{\mathrm{ch}}$ values represent different power sweep measurements, and a uniform PSD over the entire bandwidth has been retained for all of these measurements. Bearing these details in mind, we therefore define the optimal value of $\overline{P}_{\mathrm{ch}}$ within the investigated range as the optimal launch power. The definition of the optimal $\overline{P}_{\mathrm{ch}}$ value is not straightforward, as distinct CUTs reach their maximum measured GSNR at different $\overline{P}_{\mathrm{ch}}$ values (the same is true considering predicted GSNRs). Considering these individual optimal $\overline{P}_{\mathrm{ch}}$ values for each CUT, we select the minimum to be the overall optimal $\overline{P}_{\mathrm{ch}}$, ensuring that all channels do not exceed their own optimal values. Given this definition, the optimal launch power for both spectral configurations is $\overline{P}_{\mathrm{ch}} =$ -0.5 dBm and $\overline{P}_{\mathrm{ch}} =$ -1 dBm, considering the set of measured and predicted GSNRs, respectively. From an application standpoint, GNPy provides a sub-optimal launch power that results in a limited reduction in the achieved GSNR – this can be quantified as the RMS deviation between the measured GSNR at $\overline{P}_{\mathrm{ch}} =$ -1 dBm and the maximum measured GSNR for each channel; for both investigated spectral configurations this metric is equal to 0.3 ± 0.1 dB.

Lastly, the comparison of the measured and predicted values of GSNR, OSNR and SNR_{NL} for all CUTs is shown in Fig. 9 for $\overline{P}_{\mathrm{ch}} =$ -0.5 dBm. It is visible that the flat GSNR assumption is verified in this case, as the GSNR standard deviation for all channels is 0.2 ± 0.1 dB for both spectral configurations. As previously mentioned, the CUT with the highest symbol rate, highlighted in yellow on the the right-hand in Fig. 9, appears to experience an additional penalty that is not included in the simulation abstraction; for all other CUTs, GNPy provides a conservative estimation of the SNR_{NL}, which leads to an accurate

GSNR prediction.

Moreover, we highlight that the GSNR values do not vary significantly, with a RMS deviation of 0.1 ± 0.1 dB, when the CUT with symbol rate of 62 Gbaud is moved from the center to the edge of the sub-region of interest. This result is very important from an application standpoint as it suggests that the relative position of the large and narrow CUTs in a flex-rate framework is not significant when a constant PSD is implemented; consequently, system management and the optimization performed by the optical line controller is further simplified. We remark that this observation can be combined with the results of [38] to consider an optimal system working point which provides a flat and uniform GSNR distribution over the entire C-band.

5. CONCLUSION

In this work we experimentally validate the reliability and accuracy of GNPy as a software model for the WDM optical transport within a flex-grid flex-rate multi-vendor scenario, including various transmission data rates ranging from 100 to 300 Gbit/s and different modulation formats, including shaped constellations. To the best of our knowledge, this manuscript represents one of the first application examples of a QoT estimator implementation within a diverse transmission scenario. Looking into the back-to-back characterizations of the distinct TRXs, we further experimentally observe the unequivocal relation between the pre-FEC BER and the LP GSNR. In particular, when the GSNR is quantified over the channel bandwidths it is clear that the BER variations depend uniquely upon the specific modulation format, except for some insignificant fluctuations. Furthermore, we show that the GSNR distribution over the distinct channels is approximately flat when a constant PSD is implemented for the launch power and does not depend on the relative position of large and narrow symbol rate channels, at least in the investigated scenario. These features lead to a further simplification from optimization and management perspectives: from an application standpoint, an operator may consider a flat GSNR distribution and divide the available bandwidth in a flex-grid flex-rate framework, basing the design of the spectral configuration only on techno-economic assessments (e.g. total number of TRXs, power budget), as the total system capacity is not significantly affected by any specific choice.

In this framework, the QoT estimator provided by the GNPy engine is a valuable tool that allows the retrieval of a conservative and efficient working point – the estimated optimal launch power provided by the GNPy simulations, which is slightly sub-optimal with respect to the reachable maximum GSNR of the individual channels, however this reduction is limited to fractions of a dB. As a practical consequence, in partially disaggregated network scenarios, the OLCs controlling power levels on each ROADM-to-ROADM OLS may operate independently by setting the optimal PSD using a GNPy implementation.

FUNDING

This project has received funding from the European Union's Horizon 2020 research and innovation program under the Marie Skłodowska-Curie grant agreement 814276.

ACKNOWLEDGMENT

The authors would like to thank the OOPT-PSE working group of the Telecom Infraproject

REFERENCES

1. "Cisco visual networking index: Forecast and methodology," https://www.cisco.com/c/en/us/solutions/service-provider/visual-networking-index-vni/index.html (2018). [Online; accessed 20-January-2021].
2. "Mordor intelligence, optical transport network market - growth, trends, covid-19 impact, and forecast (2021 - 2026)," https://www.mordorintelligence.com/industry-reports/optical-transport-network-market (2021).
3. "Itu-t - g.694.1 : Spectral grids for wdm applications: Dwdm frequency grid," https://www.itu.int/rec/T-REC-G.694.1-202010-I/en (2020).
4. C. Doerr and L. Chen, "Silicon photonics in optical coherent systems," Proc. IEEE **106**, 2291–2301 (2018).
5. F. Buchali, V. Aref, R. Dischler, M. Chagnon, K. Schuh, H. Hettrich, A. Bielik, L. Altenhain, M. Guntermann, R. Schmid *et al.*, "128 gsa/s sige dac implementation enabling 1.52 tb/s single carrier transmission," J. Light. Technol. **39**, 763–770 (2020).
6. H. Sun, M. Torbatian, M. Karimi, R. Maher, S. Thomson, M. Tehrani, Y. Gao, A. Kumpera, G. Soliman, A. Kakkar *et al.*, "800g dsp asic design using probabilistic shaping and digital sub-carrier multiplexing," J. lightwave technology **38**, 4744–4756 (2020).
7. F. P. Guiomar, R. Li, C. R. Fludger, A. Carena, and V. Curri, "Hybrid modulation formats enabling elastic fixed-grid optical networks," J. Opt. Commun. Netw. **8**, A92–A100 (2016).
8. J. Cho and P. J. Winzer, "Probabilistic constellation shaping for optical fiber communications," J. Light. Technol. **37**, 1590–1607 (2019).
9. Y. Akulova, "Inp photonic integrated circuits for high efficiency pluggable optical interfaces," in *Optical Fiber Communication Conference,* (Optical Society of America, 2015), p. W3H.1.
10. E. Riccardi, P. Gunning, Ó. G. de Dios, M. Quagliotti, V. López, and A. Lord, "An operator view on the introduction of white boxes into optical networks," J. Light. Technol. **36**, 3062–3072 (2018).
11. H. Nishizawa, W. Ishida, Y. Sone, T. Tanaka, S. Kuwabara, T. Inui, T. Sasai, and M. Tomizawa, "Open whitebox architecture for smart integration of optical networking and data center technology," J. Opt. Commun. Netw. **13**, A78–A87 (2021).
12. S. Gringeri, N. Bitar, and T. J. Xia, "Extending software defined network principles to include optical transport," IEEE Commun. Mag. **51**, 32–40 (2013).
13. M. Birk, O. Renais, G. Lambert, C. Betoule, G. Thouenon, A. Triki, D. Bhardwaj, S. Vachhani, N. Padi, and S. Tse, "The openroadm initiative," IEEE/OSA J. Opt. Commun. Netw. **12**, C58–C67 (2020).
14. "Oif - 400zr," https://www.oiforum.com/technical-work/hot-topics/400zr-2/ (2020).
15. "Telecom infra project - rfi template for phoenix," https://exchange.telecominfraproject.com/rfi/phoenix (2020).
16. M. Filer, M. Cantono, A. Ferrari, G. Grammel, G. Galimberti, and V. Curri, "Multi-Vendor Experimental Validation of an Open Source QoT Estimator for Optical Networks," J. Light. Technol. **36**, 3073–3082 (2018).
17. V. Kamalov, M. Cantono, V. Vusirikala, L. Jovanovski, M. Salsi, A. Pilipetskii, D. K. M. Bolshtyansky, G. Mohs, E. R. Hartling, and S. Grubb, "The subsea fiber as a shannon channel," in *Proceedings of the SubOptic,* (2019).
18. A. Ferrari, M. Filer, K. Balasubramanian, Y. Yin, E. Le Rouzic, J. Kundrát, G. Grammel, G. Galimberti, and V. Curri, "Experimental validation of an open source quality of transmission estimator for open optical networks," in *2020 Optical Fiber Communications Conference and Exhibition (OFC),* (IEEE, 2020), pp. 1–3.
19. J. Slovak, W. Schairer, M. Herrmann, and E. Torrengo, "Determination of channel osnr and channel osnr margin at real network conditions," (2021-07-01). US Patent US2021203415A1.
20. A. Ferrari, M. Filer, K. Balasubramanian, Y. Yin, E. Le Rouzic, J. Kundrát, G. Grammel, G. Galimberti, and V. Curri, "Gnpy: an open source application for physical layer aware open optical networks," J. Opt. Commun. Netw. **12**, C31–C40 (2020).
21. V. Curri, "Software-defined wdm optical transport in disaggregated open optical networks," in *2020 22nd International Conference on*

Transparent Optical Networks (ICTON), (IEEE, 2020), pp. 1–4.
22. "GitHub repository of GNPy," DOI: 10.5281/zenodo.3458319.
23. G. Grammel, V. Curri, and J. L. Auge, "Physical simulation environment of the telecommunications infrastructure project (tip)," in *Optical Fiber Communication Conference/National Fiber Optic Engineers Conference 2018,* (2018).
24. A. Ferrari, M. Filer, K. Balasubramanian, Y. Yin, E. L. Rouzic, J. Kundrát, G. Grammel, G. Galimberti, and V. Curri, "Gnpy: an open source application for physical layer aware open optical networks," J. Opt. Commun. Netw. **12**, C31–C40 (2020).
25. A. Ferrari, K. Balasubramanian, M. Filer, Y. Yin, E. L. Rouzic, J. Kundrát, G. Grammel, G. Galimberti, and V. Curri, "Assessment on the in-field lightpath qot computation including connector loss uncertainties," J. Opt. Commun. Netw. **13**, A156–A164 (2021).
26. A. D'Amico, E. London, B. Le Guyader, F. Frank, E. Le Rouzic, E. Pincemin, N. Brochier, and V. Curri, "Gnpy experimental validation on flex-grid, flex-rate wdm optical transport scenarios," in *Optical Fiber Communication Conference,* (Optical Society of America, 2021), pp. W1G–2.
27. L. Yan, E. Agrell, M. N. Dharmaweera, and H. Wymeersch, "Joint assignment of power, routing, and spectrum in static flexible-grid networks," J. Light. Technol. **35**, 1766–1774 (2017).
28. V. Curri, A. Carena, A. Arduino, G. Bosco, P. Poggiolini, A. Nespola, and F. Forghieri, "Design strategies and merit of system parameters for uniform uncompensated links supporting nyquist-wdm transmission," J. Light. Technol. **33**, 3921–3932 (2015).
29. S. Gringeri, B. Basch, V. Shukla, R. Egorov, and T. J. Xia, "Flexible architectures for optical transport nodes and networks," IEEE Commun. Mag. **48**, 40–50 (2010).
30. C. Manso, R. Muñoz, N. Yoshikane, R. Casellas, R. Vilalta, R. Martínez, T. Tsuritani, and I. Morita, "Tapi-enabled sdn control for partially disaggregated multi-domain (ols) and multi-layer (wdm over sdm) optical networks," J. Opt. Commun. Netw. **13**, A21–A33 (2021).
31. J. Kundrát, O. Havliš, J. Jedlinskỳ, and J. Vojtěch, "Opening up roadms: let us build a disaggregated open optical line system," J. Light. Technol. **37**, 4041–4051 (2019).
32. A. Triki, E. L. Rouzic, O. Renais, G. Lambert, G. Thouenon, C. Betoule, E. Delfour, S. Vachhani, and B. Bathula, "Open-source qot estimation for impairment-aware path computation in openroadm compliant network," in *2020 European Conference on Optical Communications (ECOC),* (2020), pp. 1–3.
33. A. D'Amico, S. Straullu, G. Borraccini, E. London, S. Bottacchi, S. Piciaccia, A. Tanzi, A. Nespola, G. Galimberti, S. Swail *et al.*, "Enhancing lightpath qot computation with machine learning in partially disaggregated optical networks," IEEE Open J. Commun. Soc. **2**, 564–574 (2021).
34. E. Le Rouzic, A. Lindgren, S. Melin, D. Provencher, R. Subramanian, R. Joyce, F. Moore, D. Reeves, A. Rambaldi, P. Kaczmarek, K. Weeks, S. Neidlinger, G. Agrawal, S. Krishnamoha, B. Raszczyk, T. Uhlar, R. Casellas, O. Gonzalez de Dios, and V. Lopez, "Operationalizing partially disaggregated optical networks: An open standards-driven multi-vendor demonstration," in *2021 Optical Fiber Communications Conference and Exhibition (OFC),* (2021), pp. 1–3.
35. V. Curri, "Software-defined wdm optical transport in disaggregated open optical networks," in *2020 22nd International Conference on Transparent Optical Networks (ICTON),* (2020), pp. 1–4.
36. E. London, E. Virgillito, A. D'Amico, A. Napoli, and V. Curri, "Simulative assessment of non-linear interference generation within disaggregated optical line systems," OSA Continuum **3**, 3378–3389 (2020).
37. S. Walker, "Rapid modeling and estimation of total spectral loss in optical fibers," J. lightwave technology **4**, 1125–1131 (1986).
38. G. Borraccini, A. D'Amico, S. Straullu, A. Nespola, S. Piciaccia, A. Tanzi, G. Galimberti, S. Bottacchi, S. Swail, and V. Curri, "Cognitive and autonomous qot-driven optical line controller," J. Opt. Commun. Netw. **13**, E23–E31 (2021).
39. M. Cantono, D. Pilori, A. Ferrari, C. Catanese, J. Thouras, J.-L. Augé, and V. Curri, "On the interplay of nonlinear interference generation with stimulated raman scattering for qot estimation," J. Light. Technol. **36**, 3131–3141 (2018).
40. D. Semrau, R. I. Killey, and P. Bayvel, "The gaussian noise model in the presence of inter-channel stimulated raman scattering," J. Light. Technol. **36**, 3046–3055 (2018).
41. A. D'Amico, E. London, E. Virgillito, A. Napoli, and V. Curri, "Quality of transmission estimation for planning of disaggregated optical networks," in *2020 International Conference on Optical Network Design and Modeling (ONDM),* (IEEE, 2020), pp. 1–3.